DECEMBER 02 2025

Similarity spectra analysis of a lab-scale afterburning jet noise rig

Ashwin Kumar ; Joseph W. Meadows ; Kent L. Gee

J. Acoust. Soc. Am. 158, 4311–4320 (2025)
https://doi.org/10.1121/10.0041761

JASA ARTICLE

Similarity spectra analysis of a lab-scale afterburning jet noise rig

Ashwin Kumar,[1] Joseph W. Meadows,[1,a)] and Kent L. Gee[2]
[1]Department of Mechanical Engineering, Virginia Tech, Blacksburg, Virginia 24060, USA
[2]Department of Physics and Astronomy, Brigham Young University, Provo, Utah 86402, USA

ABSTRACT:
This paper presents the first study comparing the spectra of a lab-scale afterburning rig operating at a relevant total temperature ratios value of ∼6, typical of Full-Scale (FS) afterburning jets, against Tam's similarity model. The spectral characteristics of FS afterburning jets were successfully reproduced on a lab-scale. Far-field acoustic data at 63 diameters relative to the nozzle exit were used to fit the similarity spectra, with a priority placed on achieving the best fit for the overall shape of the measured spectra while ensuring a smooth growth or decay of the peak frequencies. The transition region, which is delineated by a narrow range of microphone locations from 90° to 107.5°, required a combination of fine-scale similarity spectra (FSS) and large-scale similarity spectra (LSS) to better model both the peaks and roll-offs of the measured spectra. Only LSS was needed to model the spectra near the region of maximum overall sound pressure level radiation, whereas sideline angles only needed FSS. The similarity model was unable to accurately predict the double peaks observed at select angles. Additionally, a mismatch in the high-frequency slope between the similarity model and the measured spectra became apparent outside the region of peak radiation. © *2025 Acoustical Society of America*. https://doi.org/10.1121/10.0041761

(Received 26 March 2025; revised 18 September 2025; accepted 9 November 2025; published online 2 December 2025)
[Editor: Con Doolan] Pages: 4311–4320

NOMENCLATURE

BSN	Broadband shock associated noise
FS	Full-scale
FSN	Fine scale noise
FSS	Fine scale similarity spectra
G	Autospectral density
LES	Large-eddy simulation
LSN	Large-scale noise
LSS	Large-scale similarity spectra
NPR	Nozzle pressure ratio
OASPL	Overall sound pressure level
SPL	Sound pressure level
Sr	Strouhal number
TTR	Total temperature ratio

I. INTRODUCTION

Supersonic jet noise reduction studies and their outcomes have a long-term impact on the hearing of US Navy personnel. Since this has been identified as a big contributor to hearing loss (Doychak, 2010), jet noise studies have been done in FS engine tests, lab-scale rig tests, and using computational fluid dynamics to better understand the mechanisms responsible for generating jet noise. The ultimate goal is to reduce jet noise without reducing engine thrust. Jet noise is generated by the interaction of turbulent eddies of the aircraft's nozzle exhaust and the quiescent air. Jet noise can be classified as either subsonic or supersonic. Supersonic jet noise can be further classified as turbulent mixing noise, broadband shock associated noise (BSN), and screech tones. Turbulent mixing noise can be further divided into two, namely, large-scale noise (LSN) and fine-scale noise (FSN). A comprehensive review of all these components has been presented by Tam (1995). In general, LSN tends to radiate at downstream/aft angles, whereas FSN tends to manifest in sidelines and upstream angles. Similarly, BSN has been observed to be dominant at upstream locations where FSN dominates (Epps *et al.*, 2020).

Using a wide range of far-field data sets of several cold and heated laboratory scale jets, which investigated the two turbulent mixing noise sources, Tam *et al.* (1996) developed an empirical similarity spectra to model LSN and FSN. This decomposition of total noise into two distinct noise components corresponds well to the findings of Schlinker (1975) and Laufer *et al.* (1976). When the frequency is normalized by the peak frequency, the LSS has a narrow peak at an abscissa of 1 with steeper slopes on either side of the peak. The FSS has a relatively broader peak with a gradual roll-off on either side of the peak. Both of these characteristics are depicted in Fig. 1, where the frequency values on the *x*-axis are normalized by the peak frequency. Although the similarity spectra models are independent of the jet operating parameters (Tam *et al.*, 1991), the relative contribution and peak frequencies of these two sources are highly dependent on jet Mach number, Total Temperature Ratio (TTR), and radiation angle (Tam *et al.*, 2008; Viswanathan, 2002). Tam *et al.* suggested that at any given radiation angle, the total spectra is the sum of LSS and FSS. These models were

a)Email: jwm84@vt.edu

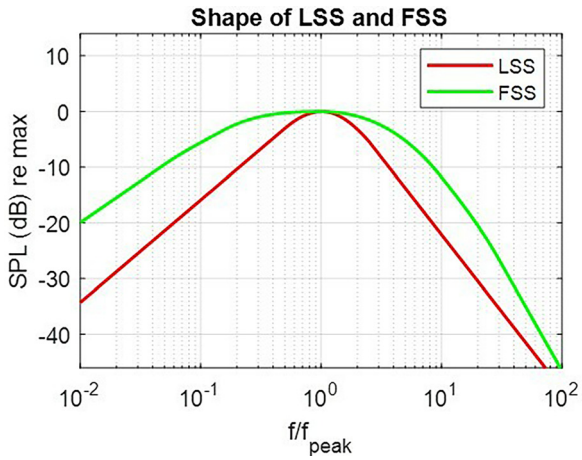

FIG. 1. Shape of LSS and FSS curves.

successfully compared against data sets from several lab-scale studies (Tam *et al.*, 1991; Viswanathan, 2002, 2004; Epps *et al.*, 2020; Tam and Zaman, 2000). In general, they provide a very good agreement for heated/unheated and subsonic/supersonic conditions. In most cases, just the FSS seems to provide a good match for the noise spectra measured at upstream and sideline angles, whereas the LSS alone provides a good match at higher downstream angles. The transition region in between required a combination of both to better predict the recorded spectra.

Neilsen *et al.* (2013a) were the first to compare the recorded spectra against the Tam *et al.* (1996) similarity spectra model at idle, intermediate, military, and afterburner conditions of the FS military jet. These data were taken from a near-field acoustical holography measurement of the F-22A by Wall *et al.* (2012). In the study by Neilsen *et al.* (2013a), the LSS and FSS of the similarity spectrum model were combined when necessary, and it showed a large degree of agreement with the measured noise spectra except for the shallower slope at high frequencies at military and afterburner conditions. It was noted that the double peak feature that appeared in the military and afterburner spectra at aft angles of the FS jet was not observed in lab-scale jets. In another study, Neilsen *et al.* (2019) decomposed the spectra of another FS military jet (F-35B) at different power levels using LSS, FSS, and the model developed by Kuo *et al.* (2015) for BSN. The errors between the models and the measured spectra were quantified using a broadband error map. In that study, FSS matched the power spectral density of upstream angles, while a combination of FSS and LSS was required to model the spectra at slightly farther downstream angles. However, LSS alone was sufficient to model the spectra at locations outside maximum radiation; at the maximum radiation location, LSS was only able to model the overall shape of the spectra, but could not account for the multiple peaks observed at afterburner conditions. In the above-mentioned two studies, emphasis was given to match the overall spectral shape of the recorded spectra, and in doing so, the model's peak was split between the observed multiple spectral peaks. The latter study, however, had an additional goal to vary the OASPL and the peak frequency smoothly over the downstream locations while striving for a best fit.

This was in contrast with the study done by Tam and Parrish (2015), where they attempted to determine if the dominant noise components of a high-performance aircraft at afterburner conditions are the same as those of a heated supersonic lab-scale jet using the data published by Nielsen *et al.* (Wall *et al.*, 2012). To determine that, Tam and Parrish overlaid the spectra of maximum radiation locations on top of each other, and the peak frequency for LSS was determined from the overlapped regions. Once the peak frequency was determined, the value was fixed for all locations. The area under the other peak was named as an additional noise component. Numerical simulations were used to bolster the argument that it is the indirect combustion noise, related to the movement of entropy waves through the nozzle, that manifested as the additional noise component.

Later, in another study, Tam *et al.* (2018) measured noise data on a F/A-18E and compared the noise spectra against the two-source model (Tam *et al.*, 1996). They found out that the spectral shape at three power levels (intermediate −80% N2, military, and afterburner) was quite similar at downstream directions (higher angles) and distinctly different from each other in upstream directions. In the afterburner condition, it was found that the characteristics of jet noise spectra differ significantly from lab-scale supersonic jets. It was identified that the "additional noise component" at higher frequencies occurred at inlet angles of 130°–140°, and at further higher angles, the "additional noise component" shifts to lower frequencies.

Recently, Epps *et al.* (2020) used the near-field data from the extensive measurements (both near-field and far-field data) taken by Leete *et al.* (2021) on a T-7A aircraft, which has a GE F-404 turbofan engine installed, and compared it against the Tam *et al.* (1996) similarity spectra and the model developed by Kuo *et al.* (2015) for BSN. The double peak behavior was observed at the afterburner and military conditions of the experimental data in this study as well. It was concluded that future comparisons will help evaluate the applicability of the similarity spectrum to full-scale tests. A comprehensive study on comparison of the similarity spectra with lab-scale jets, F-35 and F-22A (Neilsen *et al.*, 2013b) acknowledges the capability of the similarity spectra model to produce a reasonably good agreement, for sideline radiation with the FSS spectrum and the radiation around the maximum amplitude region with LSS spectrum, while falling short of predicting the double peak behavior and the shallow high-frequency slopes at afterburner conditions.

Although the similarity model was developed using low-temperature jets' (TTR < 5) far-field laboratory data, it has been demonstrated that it agrees with the measured spectra of high-temperature FS military jets, at both near-field and far-field locations, to a varying degree of success. The study presented in this paper is the first to compare a

https://doi.org/10.1121/10.0041761

lab-scale spectra, measured from an afterburning jet, operating at relevant conditions closer to FS afterburning jets. The main objective of this study is to determine how well the similarity spectra agree with the measured lab-scale jet's spectra and determine if similar discrepancies, observed between the similarity spectra and measured spectra of a FS afterburning jet, can be reproduced in a laboratory environment. This paper is organized as follows. First, a short description of the experiment facility is given, followed by the data analysis and results, where the spectral behavior at various angular locations is discussed. Finally, the similarity spectra for select angles are computed, compared against measured far-field spectra, and discussed in detail.

II. EXPERIMENT

This experiment was performed on the afterburning jet noise rig setup at Virginia Tech. A detailed description of the experimental facility is presented in Kumar *et al.* (2025). It consists of a steady-state combustor where air and fuel are mixed and ignited. The nozzle pressure ratio (NPR) and the TTR are maintained by controlling the air and fuel flow rates that were supplied by the respective facility compressors. The routed air is heated by an inline heater before being supplied to the combustor. The fuel line is split into two separate lines, the main and pilot fuel lines. The main fuel line was used to sustain combustion, and the pilot fuel line was used to improve flame stability. Pressure sensors, thermocouples, mass flow controllers, solenoid valves, flow control valves, etc., are all integrated through an instrumentation panel to connect to PXIe-1082 chassis with voltage, current, and thermocouple modules for data acquisition and rig control. A detailed description of the accuracy and make of the instruments can be found in Kumar *et al.* (2025). A CAD cross-section of the rig is shown in Fig. 2.

The rig is continuously cooled with water to facilitate steady-state operation. The combustion products are allowed to pass through a scaled-down GE F404 engine-based supersonic nozzle (GE Aerospace, Evandale, OH) with a design exit Mach number of 1.65. The rig is equipped with several different pressure sensors, thermocouples, and mass flow controllers to continuously monitor and record the engine operating parameters.

Far-field ground microphones were arranged in a circular arc of an equivalent radius of 63 nozzle diameters from the nozzle exit plane, which is considered the microphone array reference Point (MARP). The microphones were attached to a small fixture, pointed to the ground so that it is not in direct contact with the ground, and were oriented perpendicular to the line connecting the microphone and MARP. Twenty-seven GRAS 1/4″ 46BD microphones (GRAS, Holte, Denmark) were located at angular locations from 85° to 170° from the upstream inlet axis with a fine resolution of 2.5° at expected peak radiation angles and at a coarser resolution of 5° at other locations.

The microphone data were collected at a sampling rate of 204.8 kHz for about 5 min using a 24-bit National Instruments PXie-4499 DAQ module (National Instruments, Austin, TX). The picture of the supersonic nozzle and the schematic setup of the microphones are shown in Figs. 3 and 4. The operating condition for the present study had a design Mach number of 1.65, TTR of $\sim 6.0 \pm 0.09$, and a NPR of $\sim 3.33 \pm 0.031$, which corresponds to a fully expanded Mach number of 1.47 and a jet exit Reynolds number of 3×10^5.

III. DATA ANALYSIS AND RESULTS

A. Data processing

The total temperature was determined using an energy balance approach, which involves the assumptions of equilibrium combustion, all heat loss is transferred to the water cooling circuit, and the fuel composition (natural gas) as 95% CH_4, 3% C_2H_6, 1% CO_2, and 1% N_2. To process the raw microphone voltages, the "pwelch" function in MATLAB was utilized to compute the auto-Spectrum at each frequency. A Hanning window of size 20480 with a 50% overlap was applied and the resulting auto-spectrum (G) was then converted to sound pressure level (SPL) using a reference pressure of 20 μPa, as illustrated in Eq. (1). Each spectra is subtracted by 6 dB to account for the pressure doubling effect at the ground (SAE International, 1983):

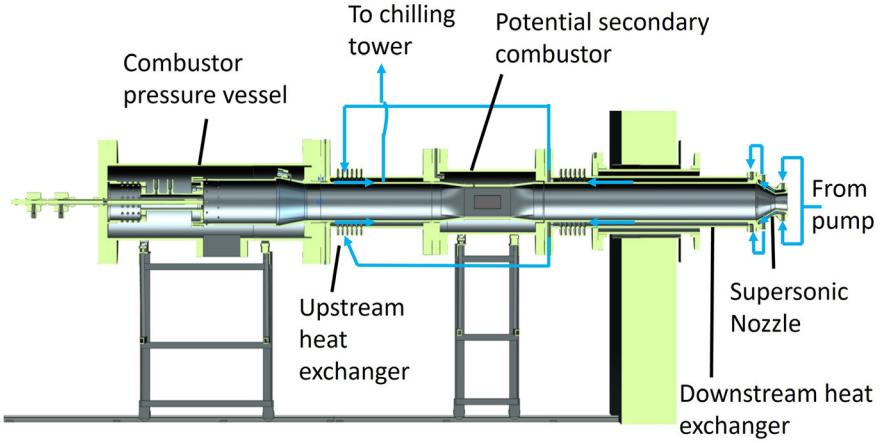

FIG. 2. CAD cross-section of the afterburning rig.

FIG. 3. Scaled-down F-404 nozzle with cooling water lines.

$$SPL(f) = 10\log_{10}\left[\frac{G(f)}{4 * (20e^{-}6)^{2}}\right]. \quad (1)$$

B. Spectral characteristics at select locations

The spectral behavior of the far-field varies considerably at each angular location. The far-field OASPL shown in Fig. 5 has been previously benchmarked and shown to match the FS aircraft's OASPL in Kumar *et al.* (2025). Figure 6 shows the spectra at select microphone locations along the polar arc. As the mic angle increases from the sidelines to downstream, a small bump-like feature starts to appear at a Strouhal number (Sr) of 0.2 at 107.5°. This feature's level increases with angle, with the slow transition of the broad peak of the sideline angles of 85° to a narrow peak. At 125°, a double peak behavior starts to appear, and

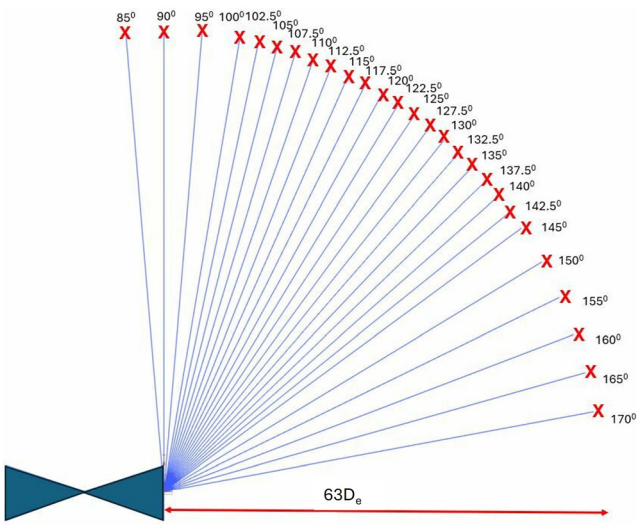

FIG. 4. Microphone arc setup schematic.

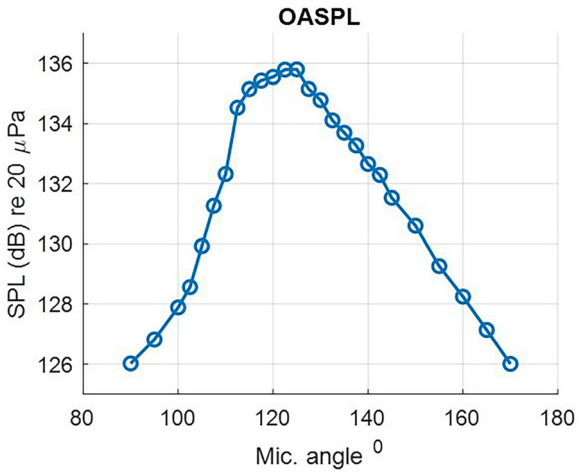

FIG. 5. Far-field OASPL.

the energy of the previously narrow peak appears to have been split between the two peaks, with the second peak at a slightly higher SPL value, and this location also happens to be the angle of peak radiation. After 130°, both peaks seem to reduce in SPL, while the second peak's magnitude of reduction is relatively greater. These double peaks are manifestations of spatio-spectral lobing effects in an angular cross-section across frequencies (Kumar *et al.*, 2025). Olaveson and Gee (2024) suggest that these lobes are a representation of rapid energy bursts concentrated at key spectral peaks, radiating with distinct directivity patterns based on their spatio-spectral, temporal analysis of lobes from T-7A acoustic measurement (Leete *et al.*, 2021). Although a definitive explanation for lobe behavior has yet to be established, evidence from multiple full-scale engine tests suggests that Mach waves and interactions between shock cells and turbulence could significantly influence this phenomenon.

Overall, moving across the angles towards the far downstream side, the SPL value at each Sr increases near the peak radiation angle and then decreases. This is observed along with the gradual decrease in peak Sr at each location from about Sr of 0.2 at 107.5° to about 0.02 at 165°. The tall narrow sharp spike shown in the spectra at about Sr 0.033 and the smaller spikes at about Sr 0.01 and 0.2 are manifestations of combustion instabilities (Kumar *et al.*, 2025). It can also be inferred that combustion instabilities also have a preferred direction of maximum radiation, which aligns closely with the OASPL directivity.

C. Similarity spectra

The similarity model equations for LSS and FSS presented in Neilsen *et al.* (2019) were used in this study. Several different methods for selecting peak frequencies of the LSS and FSS spectra have been presented in the literature, which include visual inspection and/or mathematical algorithms. As mentioned before, Tam and Parrish (2015) overlaid the spectra of peak radiation locations to determine the overlapping peak as the LSS peak frequency. Dahl and Papamoschou (2000) used a least squares fit to find great

https://doi.org/10.1121/10.0041761

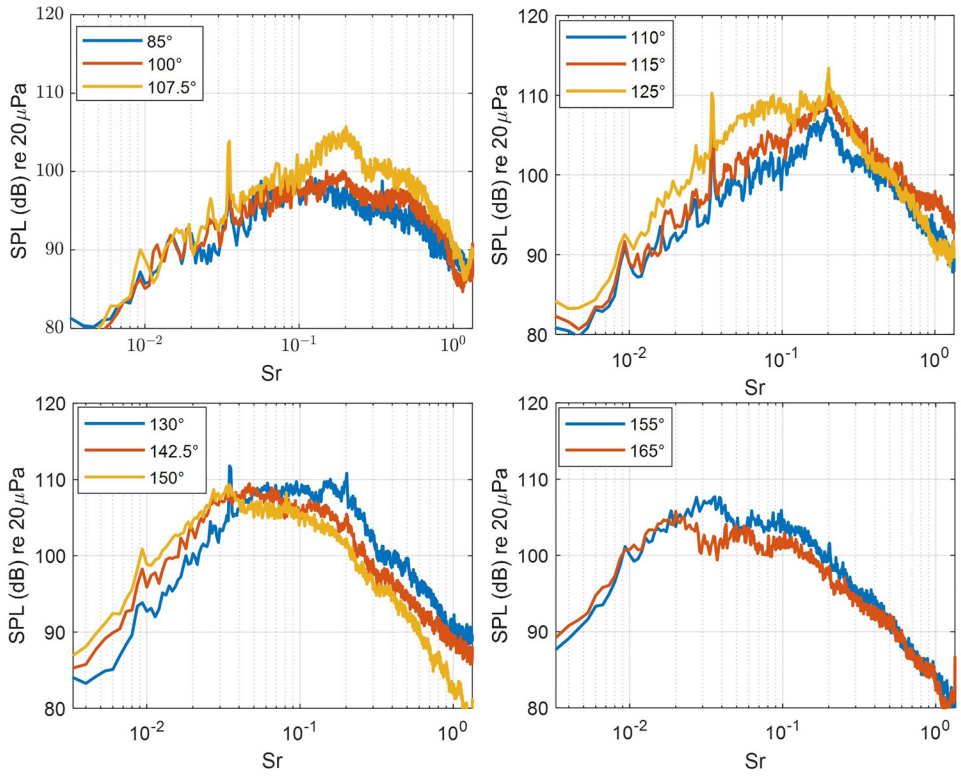

FIG. 6. Sound pressure levels at select microphone locations. Angles are relative to the jet inlet axis.

agreement between the similarity spectra and the measured spectra for heated coaxial jets. Trade-off between mutually exclusive fits for peak frequency and higher frequency slope have also been made (Tam *et al.*, 1996; Dahl and Papamoschou, 2000; Schlinker *et al.*, 2009). The approach presented here seeks to incorporate the best aspects of the studies mentioned above. Two important constraints were made for the spectral match. First, importance was given to the overall shape of the spectra rather than just matching peaks. Second, the peak frequencies of LSS were constrained to have a smooth increase or decrease over the microphone locations as suggested in reference (Neilsen *et al.*, 2019).

Initially, the OASPL at each microphone angle was determined, and the angle of peak radiation was identified. Assuming only LSS contribution at this angular location, a sub-routine was developed to find the peak frequency (Sr) using a least squares fit. Once the peak frequency (Sr) was determined, visual inspection was used to obtain the best fit for the overall curve. The same procedure is applied to the adjacent angular locations to determine the trend of the peak frequency (Sr). As expected from previous studies (Neilsen *et al.*, 2019; Epps *et al.*, 2020), a decaying trend in the peak frequency (Sr) of LSS was observed, moving from the sidelines to the downstream, in this study as well. On the other hand, the most upstream angle (85°) mic location spectra is dominated by FSS, and a separate subroutine is used to identify the peak frequency (Sr) for FSS. Once it is determined, visual inspection is used again to get the best fit for the overall shape of the curve. This procedure of using a combination of least squares fit with enforced constraint of smooth decay of peak frequency (Sr), followed by visual inspection adjustment, is repeated for all angular locations. Since all microphone locations used in this study were located on the sidelines and downstream/aft angles, BSN was not considered in this study. The trends of the peak frequencies of LSS and FSS at each microphone location are shown in Fig. 7.

Figures 8 and 9 show a comparison of measured spectra against Tam's similarity spectra at select angular locations. At 85° location, the FSS is in good agreement with the measured spectra, agreeing with observations made in the

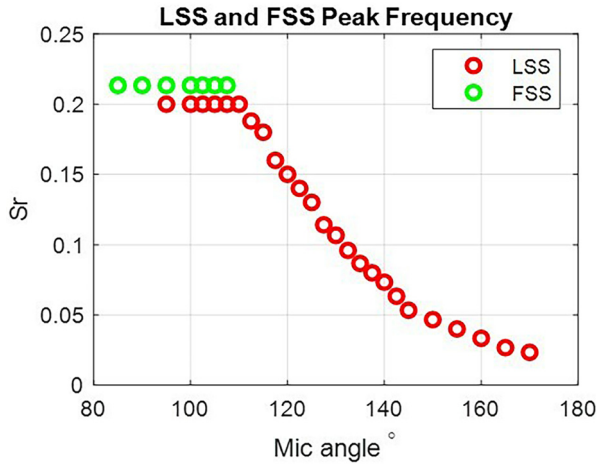

FIG. 7. LSS and FSS peak frequencies (Sr) across microphone locations.

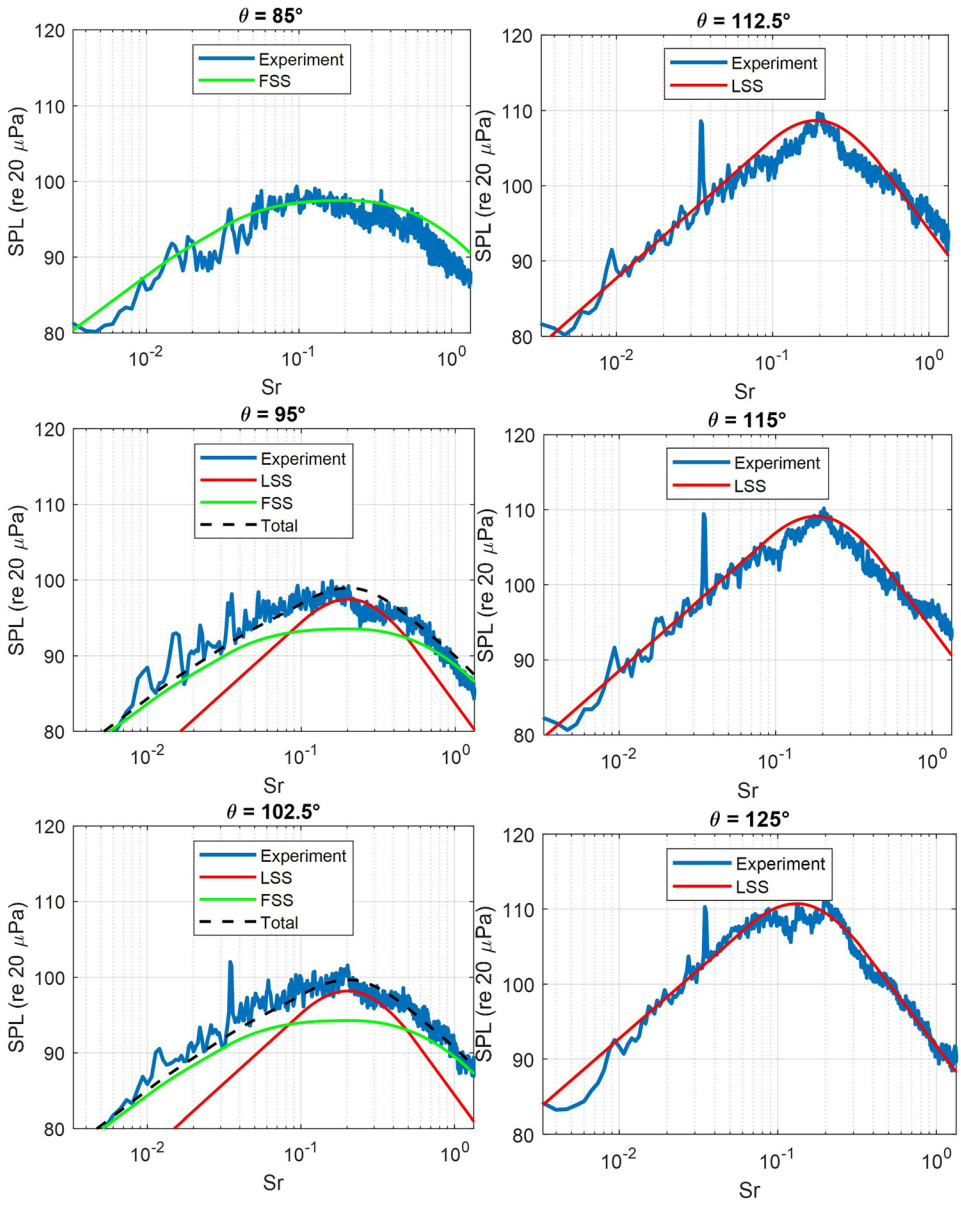

FIG. 8. Similarity spectra comparison at 85, 95, 102.5, 112.5, 115, and 125 degrees.

literature (Neilsen *et al.*, 2013a; Tam *et al.*, 1996; Epps *et al.*, 2020). The peak frequency (Sr) for FSS was ∼0.21 at this location. As the downstream angle increases, the "transition region" starts to occur around 95° (not shown here), from where a combination of LSS and FSS is required to model the total measured spectra. In that region, the peak frequency (Sr) remains constant at 0.21 for FSS and 0.20 for LSS. At about 112.5°, the "transition region" ends, and only LSS satisfies the role of modeling the total measured spectra thereafter. The LSS peak frequency (Sr) at this point is about 0.19. Thus, the combination of LSS and FSS is required for a narrow angular region of about 12 degrees from 95° until 107.5° (refer to Fig. 7). This narrow region of requirement for the LSS and FSS combination can be explained with three observations made in the literature. First, it is known that increasing the TTR moves the peak radiation angle much further upstream (Seiner *et al.*, 1992). Second, increasing the Mach number reduces the angle at which the combination of LSS and FSS is first needed (Neilsen *et al.*, 2013a). Third, an increase in jet temperature leads to a rapid completion of the transition within a narrow range of angular locations due to widening of the Mach cone (Viswanathan, 2004). Since the afterburning jet in the current study is operating at a high TTR and Mach number, the combination of the above-mentioned three phenomena causes a smaller and faster transition from FSS to LSS, with the transition beginning as far upstream as 95°. This agrees with the trend reported in the similarity study of many FS jets at afterburner conditions (Neilsen *et al.*, 2013a; Neilsen *et al.*, 2019; Epps *et al.*, 2020).

At about 125°, where the peak radiation in OASPL occurs, a split in the peak starts to appear with a small null at about Sr 0.134. As stated before, priority was given to get the best fit for the overall curve, and thus, the peak of the

https://doi.org/10.1121/10.0041761

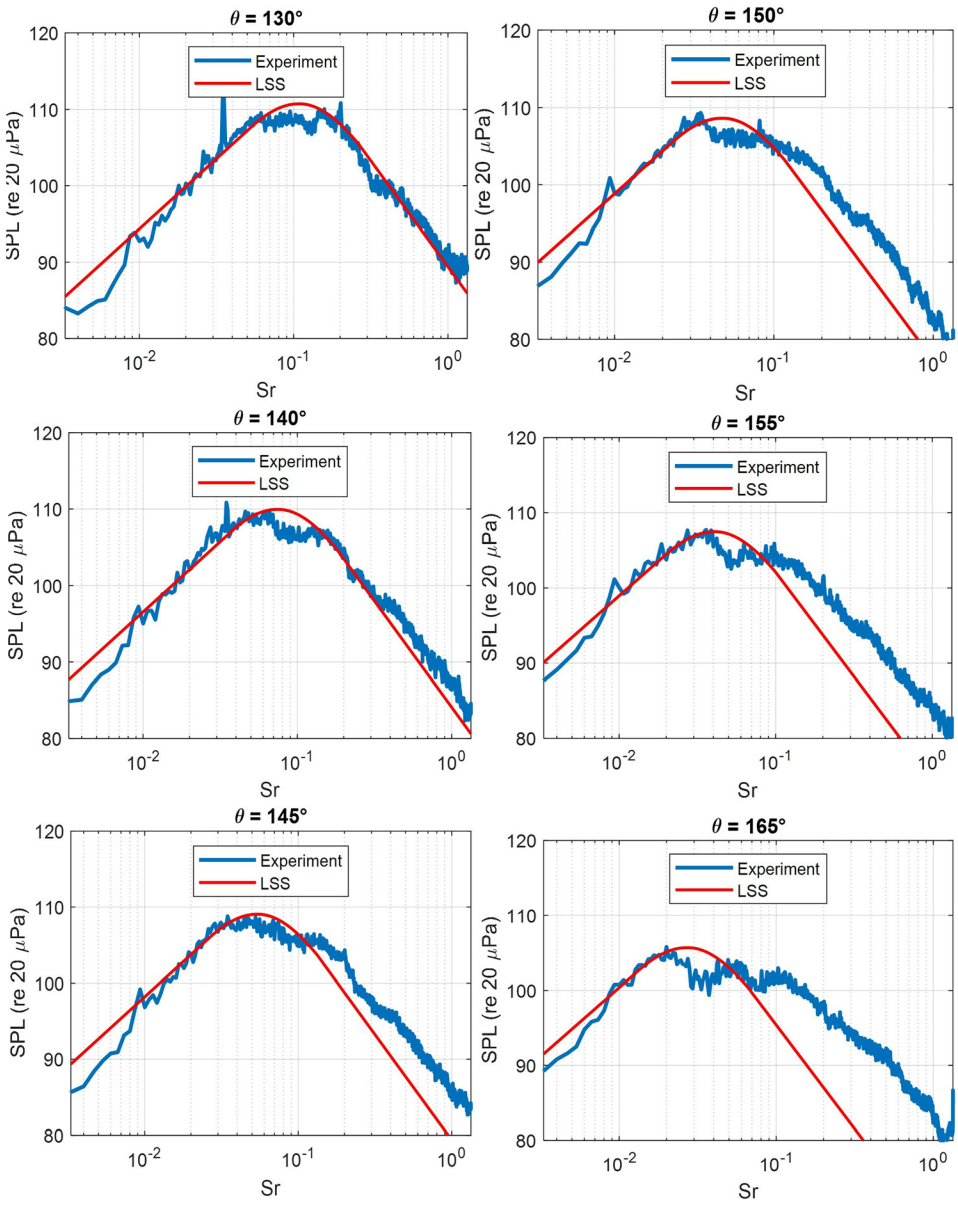

FIG. 9. Similarity spectra comparison at 130, 140, 145, 150, 155, and 165 degrees.

model is split between the two peaks of the measured spectra. Thus, the identified peak LSS frequency (Sr) at this location has gradually decreased to 0.13. At this location, the secondary peak appears to have a relatively higher SPL value than the first peak. Upon moving further downstream, at 130°, double peaks appear almost flat with both peaks around the same SPL value. At about 140°, there is a noticeable shift in the trend between the two peaks observed in the spectra. The SPL value of the second peak decreases below that of the first peak. This indicates a change in the relative magnitudes of the two peaks, with the second peak becoming lower in amplitude compared to the first peak. At this angular location, the peak LSS frequency (Sr) value has gradually decayed to 0.073. However, in general, the SPL values of both peaks gradually decrease from the onset of the double peak behavior at 125° (peak radiation angle), to the far downstream microphone locations. At 140°, the LSS model starts to show steep high-frequency roll-offs compared to the measured spectra. This mismatch between the high-frequency slopes between the LSS model and the measured spectra further worsens as the mic location increases to the farthest downstream location of 165°. This is in contrast with the observations made in the literature (Neilsen *et al.*, 2013a), where the maximum discrepancy was found in the regions of maximum radiation. Starting from 150°, the second peak starts to have a gradual flattening till 165°, at which point, the spectra appears to have more than two peaks. This observation seems to agree with literature where more than two peaks have been reported in narrow band studies of F-35 (Swift *et al.*, 2018; Wall *et al.*, 2017; Leete *et al.*, 2018). At this angular location, the LSS peak frequency (Sr) has gradually reduced to a lower value of 0.0233. Across the downstream angles, the observations made here agrees with the literature that the similarity

spectrum lacks the capability to model the double peaks in the measured spectra at afterburning conditions. Unlike the observation made in reference (Neilsen *et al.*, 2013a), at far downstream angles, it is not clear if the noise component of the high-frequency (Sr) component is caused by FSS or other sources, as fitting the FSS to such a high-frequency (Sr) would violate the approach followed where the FSS frequency is relatively constant. The method followed by Tam and Parrish (2018) fitted the LSS to the high-frequency (Sr) peak of the double peak for downstream angles, which caused the similarity spectra not to match on the low-frequency (Sr) side of the double peak. It was merely stated the low-frequency (Sr) peak is an unknown low frequency component. Future work should investigate source locations for the individual peaks to determine the actual cause of the double peaks and relative contributions from LSS/FSS/other sources. However, since the TTR/NPR values of FS military jets are generally not disclosed, establishing a correlation between acoustic and physical parameters presents a challenge. It is obvious that the similarity spectrum models are unable to account for or predict combustion noise, a common occurrence in reacting flows. While combustion instabilities have so far not been reported in FS jets, any future refinement of existing models for high TTRs should take into account this aspect of reacting flows.

Combustion/thermo-acoustic instabilities arise when pressure fluctuations and heat release fluctuations are in phase (Rayleigh criterion, see Rayleigh, 1945), and if the amplitudes grow, this could cause significant destruction to the combustor. This component of combustion noise, produced by the pressure and heat release fluctuations coupling, is called direct combustion noise. These heat release fluctuations, i.e., unsteady heat release rates, can have the consequence of uneven temperatures, also known as hot spots or entropy waves. When these entropy waves are accelerated in a varying area conduit, like a nozzle, it eventually leads to indirect combustion noise generation. A detailed description of the indirect combustion noise generation process in an accelerating environment is presented in Tam and Parrish (2018). Tam and Parrish (2015) suggested that it is the indirect combustion noise that manifests itself as the "additional noise component," observed in their spectra, and used numerical simulations to substantiate it. However, it was experimentally demonstrated for the first time that combustion instabilities can impact far-field noise spectra; although the role of indirect combustion noise versus direct combustion noise could not be independently assessed (Kumar *et al.*, 2025). Thus, this leads to the conclusion that the role and contribution of combustion noise to the overall jet noise needs to be more broadly investigated, whether it is an instability or broadband combustion noise.

IV. CONCLUSIONS

The main goal of this paper was to assess the applicability of Tam's similarity spectra model to the spectra generated by a lab-scale afterburning jet noise rig, which closely matches relevant FS jet conditions in terms of TTR and NPR. Acoustic data were collected from far-field microphones positioned in a polar arc equivalent to a radius of 63 nozzle diameters for data acquisition. Additionally, this study sought to determine whether the spectra from the lab-scale rig could reproduce similar expected discrepancies with Tam's similarity spectra, observed thus far only in FS jets operating under afterburning conditions, including twin peak behaviors and shallow high-frequency rolloffs. Furthermore, since there are no established guidelines for the application of the similarity spectra model, this paper offers a comprehensive explanation of the methodology used to conduct the similarity study. This approach combines visual inspection with mathematical algorithms to ensure accuracy and consistency. The detailed procedure outlined in this paper aims to provide a valuable reference for future researchers seeking to employ similar techniques in their studies. From this study, several key conclusions can be drawn:

- Priority was given to achieving the best fit for the overall shape of the measured spectra. Thus, at angular locations where double peaks are formed, the peak of the similarity spectrum was divided between the two. This was done while ensuring smooth growth or decay of the LSS peak frequencies over microphone locations and maintaining the FSS peak frequencies constant.
- The sideline angles only required the FSS model to fit the measured spectra. As the angle increases, the onset of the transition region occurs, where a combination of LSS and FSS is required to model the total measured spectra.
- The transition region begins and ends rapidly with a narrow range of 95° to 107.5°. This is attributed to the high Mach number and TTR value of the jet, since the high Mach number causes the onset of the transition zone earlier. The jets with high TTR result in a wider Mach cone, causing a narrow transition zone, along with moving the peak-angle radiation to farther upstream locations.
- Beyond the transition region, the general shape of the spectra begins to transform into a narrow peak at a Sr of about 0.187. Hence, only LSS was required to model the measured spectra. At about 125°, where the peak OASPL radiation occurs, double peak formation begins to occur. At this location, the SPL value of the second peak is slightly higher than that of the first peak.
- At microphone locations further-aft, the peaks appear to flatten, and the magnitude of the second peak's SPL becomes relatively lower than that of the first peak. This difference becomes more significant with increasing angular locations. The discrepancy in high-frequency slopes between the model and the measured spectra becomes apparent around the 145° location, where the measured spectra exhibit a shallow decay. This discrepancy worsens further downstream.
- Although no evidence of FSS was found at far downstream angles, more than two peaks have been observed for the first time in a lab-scale spectra at the location of 165°.
- The combustion instabilities that manifest as sharp spikes on the spectra were not accounted for by the similarity model.

Tam's similarity spectra model demonstrates a satisfactory ability to predict spectra from the sidelines up to the formation of double peaks, after which discrepancies begin to appear. These model curves were empirically derived from far-field data sets obtained from non-reacting, low-temperature jets. Although it is generally cautioned against using an empirically developed relationship beyond the range of parameter values for which it was developed, Tam's similarity spectra model has shown some success in predicting the spectra of high-temperature FS jets at different locations and conditions. However, the discrepancies observed so far have been limited to FS jets, leaving unanswered questions about whether these differences are due to unknown factors associated with FS jets or the specific operating conditions.

Since a lab-scale rig operating at relevant conditions has faithfully reproduced the same spectral behavior observed in afterburning FS jets, it becomes evident that existing similarity solutions are unable to fully reproduce the measured spectra. The authors hope that this study, along with the new capability to conduct high-temperature jet noise studies on a laboratory scale and collect datasets, will serve as a catalyst for future researchers to refine the model further. This includes addressing gaps such as modeling the onset of double peak formation and its evolution across downstream locations.

Combustion instabilities upstream of the nozzle can affect far-field spectra, although future research is needed in this area. Since operating parameters and combustion dynamics measurements can be directly synced to the acoustic measurements, future studies can shed light on the fundamental coupling between combustion noise and supersonic jet noise. This collective effort can lead to advances in understanding and developing spectral models for afterburner-relevant supersonic jet noise, paving the way for more accurate predictions and effective noise reduction strategies.

ACKNOWLEDGEMENTS

This work was sponsored by the Office of Naval Research (ONR), under Grant Nos. N00014-19-1-2430 and N00014-21-1-2069. The views and conclusions contained herein are those of the authors only and should not be interpreted as representing those of ONR, the U.S. Navy, or the U.S. Government. The authors would also like to thank Tyce Olaveson and Logan Mathews for their support during the experimental testing campaign.

AUTHOR DECLARATIONS

Conflict of Interest

The authors have no conflicts of interest to disclose.

DATA AVAILABILITY

The data that support the findings of this study are available from the corresponding author upon reasonable request.

Dahl, M. D., and Papamoschou, D. (**2000**). "Analytical predictions and measurements of the noise radiated from supersonic coaxial jets," AIAA J. **38**(4), 584–591.
Doychak, J. (**2010**). "Department of Navy jet noise reduction project overview," https://apps.dtic.mil/sti/citations/ADA553981 (Last viewed 11/21/2025).
Epps, K. A., Merrill, C. D., Vaughn, A. B., Leete, K. M., Gee, K. L., and Wall, A. T. (**2020**). "Preliminary similarity spectra analysis of noise from a high-performance trainer aircraft," Proc. Mtgs. Acoust. **42**(1), 040006.
Kumar, A., Meadows, J., Olaveson, T. W., Gee, K. L., Mathews, L. T., and Pratt, H. J. (**2025**). "Far-field noise measurements of a supersonic jet operating near afterburning conditions," Aerosp. Sci. Technol. **157**, 109842.
Kuo, C.-W., McLaughlin, D. K., Morris, P. J., and Viswanathan, K. (**2015**). "Effects of jet temperature on broadband shock-associated noise," AIAA J. **53**(6), 1515–1530.
Laufer, J., Schlinker, R., and Kaplan, R. (**1976**). "Experiments on supersonic jet noise," AIAA J. **14**(4), 489–497.
Leete, K. M., Vaughn, A. B., Bassett, M. S., Rasband, R. D., Novakovich, D. J., Gee, K. L., Campbell, S. C., Mobley, F. S., and Wall, A. T. (**2021**). "Jet noise measurements of an installed GE F404 engine," in *Proceedings of the AIAA Scitech 2021 Forum*, p. 1638.
Leete, K. M., Wall, A. T., Gee, K. L., Neilsen, T. B., James, M. M., and Downing, J. M. (**2018**). "Dependence of high-performance military aircraft noise on frequency and engine power," in *Proceedings of the 2018 AIAA/CEAS Aeroacoustics Conference*, p. 2826.
Neilsen, T. B., Gee, K. L., Wall, A. T., and James, M. M. (**2013a**). "Similarity spectra analysis of high-performance jet aircraft noise," J. Acoust. Soc. Am. **133**(4), 2116–2125.
Neilsen, T. B., Gee, K. L., Wall, A. T., James, M. M., and Atchley, A. A. (**2013b**). "Comparison of supersonic full-scale and laboratory-scale jet data and the similarity spectra for turbulent mixing noise," Proc. Mtgs. Acoust. **19**(1), 040071.
Neilsen, T. B., Vaughn, A. B., Gee, K. L., Swift, S. H., Wall, A. T., Downing, J. M., and James, M. M. (**2019**). "Three-way spectral decompositions of high-performance military aircraft noise," AIAA J. **57**(8), 3467–3479.
Olaveson, T. W., and Gee, K. L. (**2024**). "Wavelet-based characterization of spatiospectrotemporal structures in F404 engine jet noise," AIAA J. **62**(11), 4399–4410.
Rayleigh, Lord (**1945**). *The Theory of Sound* (Dover Publications, Mineola, NY), Vol. 2.
SAE International (**1983**). *AIR1672, Practical Methods to Obtain Free-Field Sound Pressure Levels from Acoustical Measurements Over Ground Surfaces* (SAE International, Warrendale, PA).
Schlinker, R., Simonich, J., Shannon, D., Reba, R., Colonius, T., Gudmundsson, K., and Ladeinde, F. (**2009**). "Supersonic jet noise from round and chevron nozzles: Experimental studies," in *Proceedings of the 15th AIAA/CEAS Aeroacoustics Conference (30th AIAA Aeroacoustics Conference)*, p. 3257.
Schlinker, R. H. (**1975**). "Supersonic jet noise experiments," Ph.D. thesis, University of Southern California, Los Angeles, CA.
Seiner, J. M., Ponton, M. K., Jansen, B. J., and Lagen, N. T. (**1992**). "The effects of temperature on supersonic jet noise emission," in *Proceedings of the 14th DGLR/AIAA Aeroacoustics Conference*, pp. 295–307.
Swift, S. H., Gee, K. L., Neilsen, T. B., Wall, A. T., Downing, J. M., and James, M. M. (**2018**). "Spatiotemporal-correlation analysis of jet noise from a round nozzle high-performance aircraft," in *Proceedings of the 2018 AIAA/CEAS Aeroacoustics Conference*, p. 3938.
Tam, C., Golebiowski, M., and Seiner, J. (**1996**). "On the two components of turbulent mixing noise from supersonic jets," in *Proceedings of the Aeroacoustics Conference*.
Tam, C., Seiner, J., and Chen, P. (**1991**). "Relationship between the instability waves and noise of high-speed jets," in *Proceedings of the 29th AIAA Aerospace Sciences Meeting*.
Tam, C. K., Aubert, A. C., Spyropoulos, J. T., and Powers, R. W. (**2018**). "On the dominant noise components of tactical aircraft: Laboratory to full scale," J. Sound Vib. **422**, 92–111.
Tam, C. K., and Parrish, S. A. (**2018**). "The physical processes of indirect combustion noise generation," Int. J. Aeroacoust. **17**(1–2), 22–35.
Tam, C. K., Viswanathan, K., Ahuja, K., and Panda, J. (**2008**). "The sources of jet noise: Experimental evidence," J. Fluid Mech. **615**, 253–292.

Tam, C. K., and Zaman, K. (**2000**). "Subsonic jet noise from nonaxisymmetric and tabbed nozzles," AIAA journal **38**(4), 592–599.
Tam, C. K. W. (**1995**). "Supersonic jet noise," J. Sound Vib. **27**(1), 17–43.
Tam, C. K. W., and Parrish, S. A. (**2015**). "Noise of high-performance aircraft at afterburner," J. Sound Vib. **352**(4), 103–128.
Viswanathan, K. (**2002**). "Analysis of the two similarity components of turbulent mixing noise," AIAA J. **40**(9), 1735–1744.
Viswanathan, K. (**2004**). "Aeroacoustics of hot jets," J. Fluid Mech. **516**, 39–82.
Wall, A. T., Gee, K. L., James, M. M., Bradley, K. A., McInerny, S. A., and Neilsen, T. B. (**2012**). "Near-field noise measurements of a high-performance military jet aircraft," Noise Control Eng. J. **60**(4), 421–434.
Wall, A. T., Leete, K. M., Gee, K. L., Neilsen, T. B., James, M. M., and McKinley, R. L. (**2017**). "Preliminary investigation of multilobe fighter jet noise sources using acoustical holography," in *Proceedings of the 23rd AIAA/CEAS Aeroacoustics Conference*, p. 3520.